The universal aspect ratio of vortices in rotating stratified flows: theory and simulation

Pedram Hassanzadeh, Philip S. Marcus and Patrice Le Gal

Journal of Fluid Mechanics / Volume 706 / September 2012, pp 46 - 57
DOI: 10.1017/jfm.2012.180, Published online: 24 May 2012

J. Fluid Mech. (2012), *vol.* 706, *pp.* 46–57.
doi:10.1017/jfm.2012.180

The universal aspect ratio of vortices in rotating stratified flows: theory and simulation

Pedram Hassanzadeh[1], **Philip S. Marcus**[1]† **and Patrice Le Gal**[2]

[1] Department of Mechanical Engineering, University of California, Berkeley, CA 94720, USA

[2] Institut de Recherche sur les Phénomènes Hors Equilibre, UMR 7342, CNRS - Aix-Marseille Université, 49 rue F. Joliot Curie, 13384 Marseille, CEDEX 13, France

(Received 19 January 2012; revised 28 February 2012; accepted 30 March 2012; first published online 25 May 2012)

We derive a relationship for the vortex aspect ratio α (vertical half-thickness over horizontal length scale) for steady and slowly evolving vortices in rotating stratified fluids, as a function of the Brunt–Väisälä frequencies within the vortex N_c and in the background fluid outside the vortex $\bar{N}$, the Coriolis parameter f and the Rossby number Ro of the vortex: $\alpha^2 = Ro(1 + Ro)f^2/(N_c^2 - \bar{N}^2)$. This relation is valid for cyclones and anticyclones in either the cyclostrophic or geostrophic regimes; it works with vortices in Boussinesq fluids or ideal gases, and the background density gradient need not be uniform. Our relation for α has many consequences for equilibrium vortices in rotating stratified flows. For example, cyclones must have $N_c^2 > \bar{N}^2$; weak anticyclones (with $|Ro| < 1$) must have $N_c^2 < \bar{N}^2$; and strong anticyclones must have $N_c^2 > \bar{N}^2$. We verify our relation for α with numerical simulations of the three-dimensional Boussinesq equations for a wide variety of vortices, including: vortices that are initially in (dissipationless) equilibrium and then evolve due to an imposed weak viscous dissipation or density radiation; anticyclones created by the geostrophic adjustment of a patch of locally mixed density; cyclones created by fluid suction from a small localized region; vortices created from the remnants of the violent breakups of columnar vortices; and weakly non-axisymmetric vortices. The values of the aspect ratios of our numerically computed vortices validate our relationship for α, and generally they differ significantly from the values obtained from the much-cited conjecture that $\alpha = f/\bar{N}$ in quasi-geostrophic vortices.

Key words: rotating flows, stratified flows, vortex flows

1. Introduction

Compact three-dimensional baroclinic vortices are abundant in geophysical and astrophysical flows. Examples in planetary atmospheres include the rows of cyclones and anticyclones near Saturn's *Ribbon* (Sayanagi, Morales-Juberias & Ingersoll 2010) and near 41 °S on Jupiter (Humphreys & Marcus 2007), and Jupiter's anticyclonic great red spot (Marcus 1993). In the Atlantic ocean, meddies persist for years (McWilliams 1985; Armi *et al.* 1988), and numerical simulations of the discs around protostars produce compact anticyclones (Barranco & Marcus 2005). The physics

† Email address for correspondence: pmarcus@me.berkeley.edu

that create, control and decay these vortices are highly diverse, and the aspect ratios $\alpha \equiv H/L$ of these vortices range from flat 'pancakes' to nearly round (where H is the vertical half-height and L is the horizontal length scale of the vortex). However, we shall show that the aspect ratios of the vortices all obey a universal relationship.

Our relation for α differs from previously published ones, including the often-used $\alpha = f/\bar{N}$, where f is the Coriolis parameter, $N \equiv \sqrt{-(g/\rho)(\partial\rho/\partial z)}$ is the Brunt–Väisälä frequency, g is the acceleration of gravity, z is the vertical coordinate, ρ is the density for Boussinesq flows and potential density for compressible flows; and a bar over a quantity indicates that it is the value of the unperturbed (i.e. with no vortices) background flow. We shall show that $\alpha = f/\bar{N}$ is not only incorrect by factors of 10 or more in some cases, but also that it is misleading; it suggests that α depends only on the background flow and not on the properties of the vortex, so that all vortices embedded in the same flow (e.g. in the Atlantic or in the Jovian atmosphere) have the same α. We shall show that this is not true. Knowledge of the correct relation for α is important. For example, there has been debate over whether the colour change, from white to red, of Jupiter's anticyclone Oval BA was due to a change in its H (de Pater *et al.* 2010). Measurements of the half-heights H of planetary vortices are difficult, but H could be accurately inferred if the correct relation for α were known. We validate our relation for α with three-dimensional numerical simulations of the Boussinesq equations. A companion paper by Aubert *et al.* (2012) validates it with laboratory experiments and with observations of Atlantic ocean meddies and Jovian vortices.

2. Aspect ratio: derivation

We assume that the rotation axis and gravity are parallel and anti-parallel to the vertical z-axis, respectively. We also assume that the vortices are in approximate cyclo-geostrophic balance horizontally and hydrostatic balance vertically (referred to hereafter as CG-H balance). Necessary approximations for CG-H balance are that the vertical v_z and radial v_r velocities are negligible compared with the azimuthal one v_θ (where the origin of the cylindrical coordinate system is at the vortex centre), that dissipation is negligible and that the flow is approximately steady in time. With these approximations, the radial r and vertical z components of Euler's equation in a rotating frame are

$$\partial p/\partial r = \rho v_\theta (f + v_\theta/r) \quad \text{and} \quad \partial p/\partial z = -\rho g, \tag{2.1}$$

where p is the pressure. We have assumed that the vortex is axisymmetric, but we show later numerically in § 7 that this approximation can be relaxed. Following the convention, we ignored the centrifugal term $\rho f^2 r/4\hat{\boldsymbol{r}}$ in (2.1) by assuming that the centrifugal buoyancy is much smaller than the gravitational buoyancy, i.e. that the rotational Froude number $f^2 d/(4\ \mathrm{g}) \ll 1$, where d is the characteristic distance of the vortex from the rotation axis (see e.g. Barcilon & Pedlosky 1967). The θ-component of Euler's equation, continuity equation, and the equation governing the dissipationless transport of (potential) density are all satisfied by a steady, axisymmetric flow with $v_r = v_z = 0$. As a consequence, (2.1) are the only equations that need to be satisfied for both Boussinesq and compressible flows. Thus, our relation for α will also be valid for both of these flows. Far from the vortex, where $\boldsymbol{v} = 0$, $p = \bar{p}$ and $\rho = \bar{\rho}$, equation (2.1) reduces to

$$\partial\bar{p}/\partial r = 0 \quad \text{and} \quad \partial\bar{p}/\partial z = -\bar{\rho} g \tag{2.2}$$

showing that $\bar{p}$ and $\bar{\rho}$ are only functions of z. Subtracting (2.2) from (2.1):

$$\partial\tilde{p}/\partial r = \rho v_\theta (f + v_\theta/r) \tag{2.3}$$

$$\partial\tilde{p}/\partial z = -\tilde{\rho} g \tag{2.4}$$

where $\tilde{p} \equiv p - \bar{p}$ and $\tilde{\rho} \equiv \rho - \bar{\rho}$ are the pressure and density anomalies, respectively. The centre of a vortex ($r = z = 0$) is defined as the location on the z-axis where $\tilde{p}$ has its extremum, so (2.4) shows that at the vortex centre (denoted by a c subscript) $\tilde{\rho}_c = 0$ or $\rho_c = \bar{\rho}(0) \equiv \rho_o$. At the vortex boundary and outside the vortex, where v_θ and $\tilde{\rho}$ are negligible, (2.3) and (2.4) show that $\tilde{p} \simeq 0$.

We define the pressure anomaly's characteristic horizontal length scale (i.e. radius) as $L \equiv \sqrt{|4\tilde{p}_c/(\nabla_\perp^2 \tilde{p})_c|}$, where the subscript $\perp$ means horizontal component. Integrating (2.3) from the vortex centre to its side boundary at $(r, z) = (L, 0)$ approximately yields

$$-\tilde{p}_c/L = \rho_o V_\theta (f + V_\theta/R_v) \tag{2.5}$$

where in the course of integration, ρ has been replaced with ρ_o, which is exact for Boussinesq flows and an approximation for fully compressible flows. Here V_θ is the characteristic peak azimuthal velocity and R_v is the approximate radius where the velocity has that peak. The analytical and numerically simulated vortices discussed below, meddies and the laboratory vortices examined by Aubert *et al.* (2012) all have $R_v \approx L$, but hollow vortices with quiescent interiors have $R_v \neq L$. For example, the Great Red Spot has $R_v \simeq 3L$ (Shetty & Marcus 2010). Similarly, integrating (2.4) from the vortex centre to its top boundary at $(r, z) = (0, H)$ approximately gives

$$\tilde{p}_c/H = g\tilde{\rho}(r = 0, z = H), \tag{2.6}$$

where H is the pressure anomaly's characteristic vertical length scale (i.e. half-height), $H \equiv \sqrt{|2\tilde{p}_c/(\partial^2\tilde{p}/\partial z^2)_c|}$.

Equation (2.5) and (2.6) can be combined to eliminate $\tilde{p}_c$:

$$\frac{\rho_o V_\theta (f + V_\theta/R_v)}{H} = -\frac{g\tilde{\rho}(r = 0, z = H)}{L}. \tag{2.7}$$

Note that this equation is basically the thermal wind equation, with the cyclostrophic term included (i.e. the gradient-wind equation (Vallis 2006)), integrated over the vortex. Using the first term of a Taylor series, we approximate $\tilde{\rho}(r = 0, z = H)$ on the right-hand side of (2.7) with

$$\tilde{\rho}(r = 0, z = H) = \tilde{\rho}_c + H\,(\partial\tilde{\rho}/\partial z)_c = H[(\partial\rho/\partial z)_c - (\partial\bar{\rho}/\partial z)_c] = \rho_o H(\bar{N}^2 - N_c^2)/g \tag{2.8}$$

where $\tilde{\rho} \equiv \rho - \bar{\rho}$ and $\tilde{\rho}_c = 0$ have been used. Note that, in general, $\bar{N}(z)$ is a function of z; however, the only way in which $\bar{N}(z)$ is used in this derivation (or anywhere else in this paper) is at $z = 0$ for evaluating $(\partial\bar{\rho}/\partial z)_c$. Therefore, rather than using the cumbersome notation $\bar{N}_c$, we simply use $\bar{N}$.

Using (2.8) in (2.7) gives our relation for α:

$$\alpha^2 \equiv \left(\frac{H}{L}\right)^2 = \frac{Ro[1 + (L/R_v)Ro]}{N_c^2 - \bar{N}^2} f^2 \tag{2.9}$$

where the Rossby number defined as $Ro \equiv V_\theta/(fL)$ can be well approximated as $Ro = \omega_c/(2f)$, ω_c being the vertical component of vorticity at the vortex centre.

Defining the Burger number as $Bu \equiv (\bar{N}H/(fL))^2$, (2.9) may be rewritten as

$$[(N_c/\bar{N})^2 - 1]Bu = Ro(1 + (L/R_v)Ro). \tag{2.10}$$

Equation (2.9) shows that α depends on two properties of the vortex: Ro and the difference between the Brunt–Väisälä frequencies inside the vortex (i.e. N_c^2) and outside the vortex (i.e. $\bar{N}^2$). Note that to derive relation (2.9), no assumption has been made on the compressibility of the flow, Rossby number smallness, dependence of $\bar{N}$ on z, or the magnitude of $N_c/\bar{N}$. Therefore, (2.9) is applicable to Boussinesq, anelastic (Vallis 2006), and fully compressible flows, cyclones (i.e. $Ro > 0$) and anticyclones (i.e. $Ro < 0$), and geostrophic and cyclostrophic flows. In the cyclostrophic limit (i.e. $|Ro| \gg 1$) with $N_c = 0$ and $R_V = L$, $Ro\,(1 + Ro) \to Ro^2$, hence (2.9) becomes $V_\theta = H\bar{N}$, agreeing with the findings of Billant & Chomaz (2001) and others. Equation (2.9) is easily modified for use with discrete layers of fluid rather than a continuous stratification, and in that case agrees with the work of Nof (1981) and Carton (2001).

Equation (2.9) has several consequences for equilibrium vortices. For example, because the right-hand side of (2.9) must be positive, cyclones must have $N_c^2 \geqslant \bar{N}^2$. Another consequence is that anticyclones with $-Ro < R_v/L$ must have $N_c^2 \leqslant \bar{N}^2$ and anticyclones with $-Ro > R_v/L$ have $N_c^2 \geqslant \bar{N}^2$. In addition, (2.9) is useful for astrophysical and geophysical observations of vortices in which some of the vortex properties are difficult to measure. For example, N_c is difficult to measure in some ocean vortices (Aubert *et al.* 2012), and H is difficult to determine in some satellite observations of atmospheric vortices (de Pater *et al.* 2010), but their values can be inferred from (2.9).

Note that N_c is a measure of the mixing within the vortex; if the density is not mixed with respect to the background flow, then $N_c \to \bar{N}$ (and the vortex is a tall, barotropic Taylor column); if the density is well mixed within the vortex so the (potential) density is uniform inside the vortex, then $N_c \to 0$ (as in the experiments of Aubert *et al.* (2012)); if $N_c^2 > \bar{N}^2$ (as required by cyclones), then the vortex is more stratified than the background flow.

3. Previously proposed scaling laws

Other relations for α that differ from our (2.9) have been published previously, and the most frequently cited one is $\alpha \equiv H/L = f/\bar{N}$. This relationship is inferred from Charney's equation for the quasi-geostrophic (QG) potential vorticity (equation (8) in Charney 1971) that was derived for flows with $|Ro| \ll 1$ and $N_c/\bar{N} \simeq 1$. Separately re-scaling the vertical and horizontal coordinates of the potential vorticity equation, and then assuming that the vortices are isotropic in the re-scaled (but not physical) coordinates, one obtains the alternative scaling $\alpha = f/\bar{N}$. Numerical simulations of the QG equation for some initial conditions have produced turbulent vortices with $H/L \approx f/\bar{N}$ (cf. Dritschel, Juarez & Ambaum 1999; McWilliams, Weiss & Yavneh 1999; Reinaud, Dritschel & Koudella 2003), even though significant anisotropy in the re-scaled coordinates was observed in similar simulations (McWilliams, Weiss & Yavneh 1994). The constraints under which the QG equation is derived are very restrictive; for example, none of the meddies or laboratory vortices studied by Aubert *et al.* (2012) meet these requirements because $N_c/\bar{N}$ is far from unity. Therefore, it is not surprising that none of these vortices, including the laboratory vortices, agree with $\alpha \approx f/\bar{N}$, but instead have α in accord with relation (2.9) (Aubert *et al.* 2012).

The constraints under which our (2.9) for α is derived are far less restrictive than those used in deriving Charney's QG equation (and we never need to assume isotropy).

In particular, one of several constraints needed for deriving Charney's QG equation is the scaling required for the potential temperature (his equation (3)), which written in terms of the potential density is

$$\tilde{\rho}/\bar{\rho} = -(f/g)(\partial\psi/\partial z), \tag{3.1}$$

where ψ is the stream function of horizontal velocity. This constraint alone (which is effectively the thermal wind equation) implies our relationship (2.9) for α. To see this, in (3.1) replace ψ with $V_\theta L$, $\partial/\partial z$ with $1/H$, V_θ with $RofL$ and $\tilde{\rho}/\bar{\rho}$ with $H\{(\partial\rho/\partial z)_c - (\partial\bar{\rho}/\partial z)\}/\bar{\rho} = (H/g)(\bar{N}^2 - N_c^2)$. With these replacements, (3.1) immediately gives

$$(H/L)^2 = Rof^2/(N_c^2 - \bar{N}^2), \tag{3.2}$$

which is the small Ro limit of (2.9).

Gill (1981) also proposed a relationship for α that differs from ours. He based his relation for α on a model two-dimensional zonal flow (that is, not an axisymmetric vortex, but rather a two-dimensional vortex) and found that α was proportional to $Rof/\bar{N}$. To determine α, Gill derived separate solutions for the flow inside and outside his two-dimensional model vortex, which he assumed was dissipationless and in geostrophic and hydrostatic balance. Despite the fact that Gill's published relation for α, obtained from the outside solution, differs from ours, we can show that his solution for the flow inside his two-dimensional vortex satisfies our scaling relation for α: Gill's solution for the zonal velocity (which is in the y-direction) is $v = -(f/a)x$ (his equation (5.14) in dimensional form). His density anomaly is $\tilde{\rho} = \rho_o(\bar{N}^2/g)z$ (i.e. within the two-dimensional vortex, $\rho = \rho_o$). The equation for v gives $\omega_z = -(f/a)$ and therefore $Ro \equiv \omega_c/(2f) = -1/(2a)$. Substituting v and $\tilde{\rho}$ into the equations for geostrophic and hydrostatic balance, gives $\partial\tilde{p}/\partial x = -\rho_o(f^2/a)x$ and $\partial\tilde{p}/\partial z = -\rho_o\bar{N}^2 z$, respectively. Using the definitions of H and L from § 2 along with $Ro = -1/(2a)$, we obtain $\alpha^2 = -Rof^2/\bar{N}^2$, which is our relation (2.9) in the limit of small Ro, $L = R_v$ and $N_c = 0$ (which are the constraints under which Gill's solution is obtained). Gill's scaling for α is derived from the flow outside the vortex, which he derived by requiring that both the tangential velocity and density are continuous at the interface between the inside and outside solutions. In general, this over-constrains the dissipationless flow (which only requires pressure and normal velocity to be continuous, see for example the vortex solution in Aubert *et al.* (2012) in which the pressure and normal component of the velocity are continuous at the interface, but not the density or tangential velocity). The extra constraints force the solution outside Gill's vortex to have additional (unphysical) length scales, resulting in Gill's relation for α differing from ours. Aubert *et al.* (2012) show that Gill's relationship for α does not fit their laboratory experiments, meddies or Jovian vortices. We examine the accuracy of both Charney's and Gill's relationships in § 7.

4. Gaussian solution to the dissipationless Boussinesq equations

It is possible to find closed-form solutions to the steady, axisymmetric, dissipationless Boussinesq equations (e.g. Aubert *et al.* 2012). One solution that we shall use to generate initial conditions for our initial-value codes is the Gaussian vortex with $\tilde{p} = \tilde{p}_c \exp[-(z/H)^2 - (r/L)^2]$ and $v_r = v_z = 0$ (where $\tilde{p}_c$, H and L are arbitrary constants). Then, $\tilde{\rho}$ is found from $\partial\tilde{p}/\partial z$ using (2.4), and v_θ is found from $\partial\tilde{p}/\partial r$ using (2.3) with ρ replaced by ρ_o. This Gaussian vortex exactly obeys our relationship (2.9) for α when the Rossby number is defined as before as $Ro \equiv \omega_c/(2f)$, when R_v is set

equal to L, and when the vertical and horizontal scales are defined as in § 2. Note that $N(r, z)$ within the vortex is not uniform, that $N_c^2 = \bar{N}^2 - 2\tilde{p}_c/(\rho_o H^2)$ and that the vortex is shielded. By shielded, we mean that there is a ring of cyclonic (anticyclonic) vorticity around the anticyclonic (cyclonic) core in each horizontal plane, and therefore at each z, circulation due to the vertical component of the vorticity is zero (i.e. the vortices are isolated). The Gaussian vortex could be a cyclone or an anticyclone depending on the choice of constants. This vortex is well studied and has been widely used to model isolated vortices, especially in the oceans (e.g. Gent & McWilliams 1986; Morel & McWilliams 1997; Stuart, Sundermeyer & Hebert 2011).

5. Numerical simulation of the Boussinesq equations

To use three-dimensional numerical simulations to verify our relation (2.9) for α in a Boussinesq flow with constant $\bar{N}$ and f, we solve the equations of motion in a rotating-frame in Cartesian coordinates (Vallis 2006):

$$\boldsymbol{\nabla}\cdot\boldsymbol{v} = 0, \quad \frac{\mathrm{D}\boldsymbol{v}}{\mathrm{D}t} = -\frac{\boldsymbol{\nabla}p}{\rho_o} + \boldsymbol{v}\times f\hat{\boldsymbol{z}} - \frac{\tilde{\rho}}{\rho_o}g\hat{\boldsymbol{z}} + \nu\nabla^2\boldsymbol{v}, \quad \frac{\mathrm{D}\tilde{\rho}}{\mathrm{D}t} = \rho_o\frac{\bar{N}^2}{g}w - \frac{\tilde{\rho}}{\tau_{rad}}, \quad (5.1)$$

where $\mathrm{D}/\mathrm{D}t = \partial/\partial t + \boldsymbol{v}\cdot\boldsymbol{\nabla}$, and $\boldsymbol{v} = (u, v, w)$. (Note that throughout this paper, we use v_z and w for the vertical component of velocity in the cylindrical and Cartesian coordinates, respectively.) We include kinematic viscosity ν in (5.1), but neglect the diffusion of density because diffusion is slow (e.g. for salt water the Schmidt number is ∼700). Instead, inspired by astrophysical vortices (e.g. Jovian vortices or vortices of protoplanetary discs) for which thermal radiation is the main dissipating mechanism, we have added the damping term $-\tilde{\rho}/\tau_{rad}$ to the density equation in (5.1) to model radiative dissipation, where τ_{rad} is radiative dissipation time scale.

A pseudo-spectral method with 256^3 modes is used to solve (5.1) in a triply periodic domain (which was chosen to be 10–20 times larger than the vortex in each direction). Details of the numerical method is the same as Barranco & Marcus (2006). The results of our triply periodic code are qualitatively, and in most cases quantitatively, the same as solutions we obtained with a code with no-slip vertical boundary conditions. That is because our vortices are far from the vertical boundaries, and therefore the Ekman circulation is absent.

6. Numerical results for vortex aspect ratios

As shown in table 1, we have examined the aspect ratios of vortices in four types of initial-value numerical experiments. The goal of these simulations is to determine how well the aspect ratios α of vortices obey our relation (2.9) as they evolve in time.

6.1. *Case A: run-down experiments*

In this case, our initial condition is the velocity and density anomaly of the Gaussian vortex from § 4 that is an exact equilibrium of the dissipationless Boussinesq equations with constant f and $\bar{N}$. These are 'run-down' experiments because they are carried out either with radiative dissipation (i.e. finite τ_{rad}) or viscosity, but not both. Owing to the weak dissipation, the vortices slowly evolve (decay) and do not remain Gaussian. Also, as a result of the dissipation (and decay), a weak secondary flow is induced (i.e. non-zero v_r and v_z).

Case	$\bar{N}/N_c$	H/L	Ro	$E_k(10^{-5})$	Case	$\bar{N}/N_c$	H/L	τ_{rad}	Ro	$E_k(10^{-5})$
A1	1/0	16/8	−0.2	25	A18	3.33/3.17	1.44/0.72	∞	−0.22	4
A2	1/0	16/8	−0.2	12.5	A19	10/10.5	0.16/0.08	∞	+0.87	250
A3	1/0	16/8	−0.2	6.25	A20	3.33/3.49	1.44/0.72	1656	+0.14	0
A4	1/0.5	16/8	−0.14	25	A21	1/1.0475	16/8	1656	+0.015	0
A5	1/0.5	4/2	−0.14	25	A22	3.33/3.17	1.44/0.72	1237	−0.22	0
A6	20/19.99	0.05/0.02	−0.11	500	A23	3.33/3.49	1.44/0.72	120	+0.14	0
A7	1/0	20/12	−0.12	11.1	A24	3.33/3.17	1.44/0.72	120	−0.22	0
A8	1/0	16/8	−0.2	25	B1	1/0	20/12	∞	−0.12	4
A9	1/0	12/12	−0.04	11.1	B2	1/0	20/12	∞	−0.12	4
A10	20/19.9	0.03/0.03	−0.2	222.2	B3	1/0	20/12	∞	−0.12	0
A11	20/19.9	0.03/0.03	−0.2	11.1	C1	1/0.761	6.09/5.67	∞	+0.33	49.7
A12	3.53/2.5	0.96/0.96	−0.5	39.3	C2	1/0.709	5.91/5.67	∞	+0.35	45.9
A13	3.54/3.45	0.96/0.96	−0.023	39.3	D1	2.5/2.5	40/2	∞	−0.75	25.4
A14	1.56/1.64	6.55/3.28	+0.0386	3.91	D2	2.5/2.5	40/2	∞	−0.75	12.7
A15	0.5/0.75	16/8	+0.0477	4	D3	1.67/1.67	90/4.5	∞	−0.5	16.9
A16	0.5/0.55	16/8	+0.0083	4	D4	5/5	10/0.5	∞	−1	50.7
A17	3.33/3.49	1.44/0.72	+0.15	4	D5	20/20	0.6/0.03	∞	+0.8	24.4

TABLE 1. Parameters of the background flows and of the vortices at the 'initial' time. For cases A, B and D the 'initial' time is $t = 0$, and for case C the 'initial' time is $t = t_{off}$. All values are in CGS units. For all cases, $f = 5$ rad s^{-1}, $g = 980$ m s^{-2} and $\rho_o = 1$ g cm^{-3}. The Ekman number is defined as $E_k \equiv \nu/(fL^2)$. See the text for the difference between cases B1 and B2. For case C1, $t_{off} = 60$ s and $Q = -64$ cm^3 s^{-1} and for case C2, $t_{off} = 30$ s and $Q = -128$ cm^3 s^{-1}.

6.2. *Case B: vortices generated by geostrophic adjustment*

This case is motivated by vortices produced from the geostrophic adjustment of a locally mixed patch of density, e.g. generated from diapycnal mixing (see e.g. McWilliams 1988; Stuart *et al.* 2011). Our flow is initialized with $\boldsymbol{v} = 0$ and $\tilde{\rho} \neq 0$. For cases B1 and B3 the initial $\tilde{\rho}$ is that of the Gaussian vortex discussed in § 4. But here, the initial flow is far from equilibrium because $\boldsymbol{v} \equiv 0$. In case B2, the initial $\tilde{\rho}$ is Gaussian in r, but has a top-hat function in z (for this case, the initial H is defined as the half-height of the top-hat function). It is observed in the numerical simulations that geostrophic adjustment quickly produces shielded vortices.

6.3. *Case C: cyclones produced by suction*

Injection of fluid into a rotating flow generates anticyclones (Aubert *et al.* 2012), while suction produces cyclones. We simulate suction by modifying the continuity equation in (5.1) as $\boldsymbol{\nabla} \cdot \boldsymbol{v} = Q(\boldsymbol{x}, t)$ where Q is a specified suction rate function. The flow is initialized with $\boldsymbol{v} = \tilde{\rho} = 0$. Suction starts at $t = 0$ over a spherical region with radius of 6 cm and is turned off at time t_{off}. A shielded cyclone is produced and strengthened during the suction process. As mentioned at the end of § 2, for $Ro > 0$, relation (2.9) requires the flow to be superstratified (i.e. $N_c > \bar{N}$). Our numerical simulations show that the initial suction creates superstratification. Cases C1 and C2 have different suction rates and t_{off}, but the same total sucked volume of fluid, and it is observed that the produced cyclones are similar.

6.4. *Case D: vortices produced from the breakup of tall barotropic vortices*

The violent breakup of tall barotropic (z-independent) vortices in rotating stratified flows can produce stable compact vortices (see e.g. Smyth & McWilliams 1998). In case D, our flows are initialized with an unstable two-dimensional columnar vortex with $v_\theta = Rof\, r \exp(-(r/L)^2)$ and $\tilde{\rho} = 0$ (for this case, the initial H is the vertical height of the computational domain). Note that the initial columnar vortex is shielded. Noise is added to the initial velocity field to hasten instabilities. The vortex breaks up and then the remnants equilibrate to one or more compact shielded vortices (in each case, only the vortex with the largest $|Ro|$ is analysed in § 7).

7. Aspect ratio: numerical simulations

In all cases, vortices reach quasi-equilibrium and then slowly decay due to viscous or radiative dissipation except for case B3 which is dissipationless and evolves only due to geostrophic adjustment. As a result, Ro decreases, and the mixing of density in the vortex interior changes (i.e. N_c changes). Therefore, it is not surprising that the aspect ratio α also changes in time. Quasi-equilibrium is reached in case A almost immediately. In case B, vortices quickly form and come to quasi-equilibrium after geostrophic adjustment. Quasi-equilibrium is achieved following the geostrophic and hydrostatic adjustments after t_{off} in case C, and (much longer) after the initial instabilities in case D.

For each case, we use the results of the numerical simulations to calculate $Ro(t) \equiv \omega_c(t)/(2f)$ and $N_c(t) \equiv \sqrt{\bar{N}^2 - g\,(\partial\tilde{\rho}(t)/\partial z)_c\,/\rho_o}$. We compute $L(t)$ and $H(t)$ from the numerical solutions using their definitions given in § 2. Calculating L based on $\boldsymbol{\nabla}_\perp^2$ rather than just r-derivatives is useful for non-axisymmetric vortices. For example, due to a small non-axisymmetric perturbation added to the initial condition of case A8, the vortex became unstable and produced a tripole (Van Heijst & Kloosterziel 1989). Cases C1 and C2 also produced non-axisymmetric vortices. We

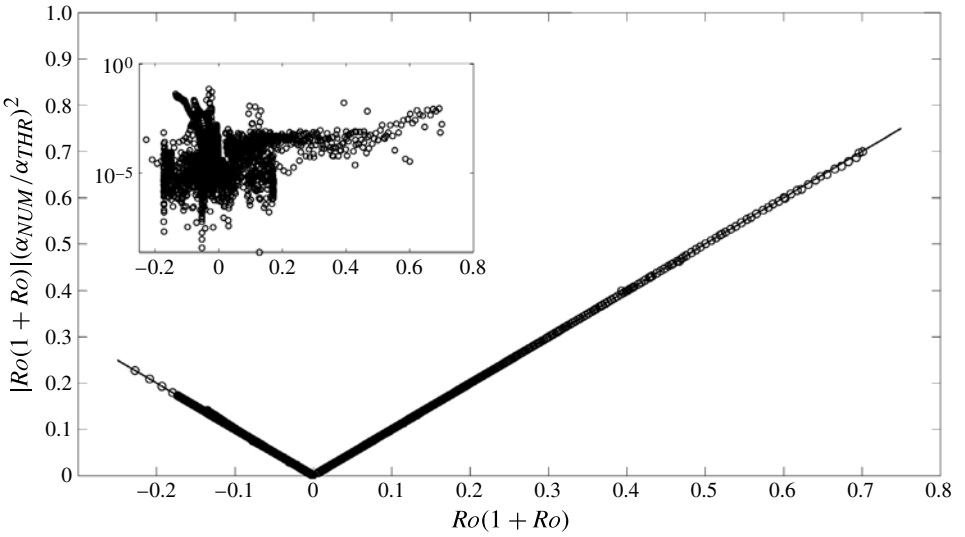

FIGURE 1. Comparison of α_{NUM} with α_{THR} (see the text for definitions). The circles show the value of $|Ro(1+Ro)|\,(\alpha_{NUM}/\alpha_{THR})^2$ and the straight lines show the value of this expression if $\alpha_{NUM} \equiv \alpha_{THR}$. All 4122 data points (circles) collapse on the straight lines (and densely cover them), validating our (2.9). Data points are recorded one inertial period ($=4\pi/f$) after the initial time (as defined in table 1) in cases A–C, and 50 inertial periods after $t = 0$ in case D. Note that all of our simulated vortices have $L = R_v$. The horizontal axis in the inset is the same as in the main figure; the inset's vertical axis is the relative difference $|1 - (\alpha_{NUM}/\alpha_{THR})^2|$ (which is <0.07). (Note that the left-most plotted point has $Ro(1+Ro) \simeq -0.25$ due to the mathematical tautology that $Ro(1+Ro) \geqslant -0.25$ for all values of Ro.)

define the numerical aspect ratio as $\alpha_{NUM}(t) \equiv H(t)/L(t)$. We define the theoretical aspect ratio α_{THR} from (2.9) using $Ro(t)$ and $N_c(t)$ extracted from the numerical results and the (constant) values of f and $\bar{N}$.

Figure 1 shows how well α_{THR} agrees with α_{NUM}. The inset in figure 1 shows that the relative difference between the two values, calculated as $|1 - (\alpha_{NUM}/\alpha_{THR})^2|$, is smaller than 0.07. For each case, the maximum difference occurs at early times or during instabilities.

Figure 2 compares the values of α_{NUM} with α_{THR} as a function of time for six cases. The figure starts at time $t = 0$, so it includes vortices which are not in CG-H equilibrium to examine the situations for which relationship (2.9) for α may not be good due to transients. Cases A1, B1 and A20 in figure 2(a) exhibit excellent agreement with our theoretical prediction for α, while case A8 shows a small deviation starting around $t = 80(4\pi/f)$. This deviation is a result of the vortex going unstable at this time (accompanying by relatively large v_r and v_z) and forming a tripolar vortex. After the tripole comes to CG-H equilibrium, its α once again agrees with theory. As the vortices dissipate, and Ro and N_c change, α can either decrease in time (cf. case A1) or increase (cf. case A20).

Figure 2(b) shows cases D1 and D3 from time $t = 0$. The remnant vortices that formed from the violent break-up of the columnar vortices are initially far from the CG-H balance. As a result, the value of α_{THR} at these early times does not fit well with

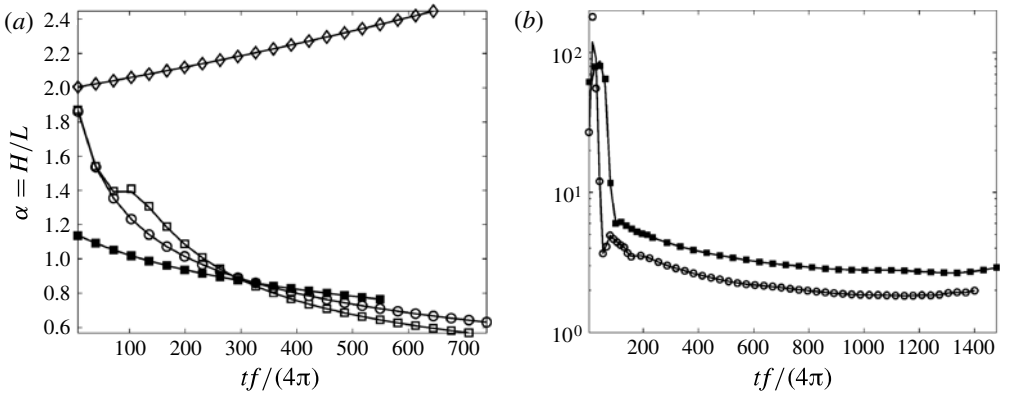

FIGURE 2. Time evolution of α_{THR} (continuous curves), and α_{NUM} for: (*a*) ∘, case A1; □, case A8; ■, case B1; and ⋄, case A20; and (*b*) ∘, case D1; and ■, case D3. Cases A1, A8 and B1 have $f/\bar{N} = 5$ and case A20 has $f/\bar{N} = 1.5$ which differ significantly from α. Case D1 has $f/\bar{N} = 2$ and case D3 has $f/\bar{N} = 3$ which agree with α only at the late times.

the values of α_{NUM}. However, after the CG-H balance is established in the remnants, our theoretical relationship (2.9) becomes valid and α_{THR} agrees well with α_{NUM}.

Figure 2(*a*) shows that the alternative scaling relation based on Charney's QG equation, $\alpha = f/\bar{N}$, is not a good fit to our numerical data. Cases A1, A8 and B1 all have $f/\bar{N} = 5$ which is obviously far from the measured aspect ratio of these vortices. Case A20 has $f/\bar{N} = 1.5$ which again does not agree with α_{NUM}. In fact, in all four cases, the difference between $\alpha_{NUM}(t)$ and $f/\bar{N}$ increases with time, while $\alpha_{THR}(t)$ always remains close to $\alpha_{NUM}(t)$. For other cases in table 1, it has been observed that for vortices which are in CG-H equilibrium, $\alpha_{NUM}/(f/\bar{N})$ can be as large as 9.56 and as small as 0.11. The data displayed in figure 2(*b*) were carefully 'cherry-picked' from all of our runs because they are unusual in that $\alpha \to f/\bar{N}$ after a long time. The fluid within the remnants strongly mixed with the background fluid, so at late times $N_c \to \bar{N}$ and *Ro* significantly decreases and therefore the conditions needed for the validity of Charney's QG equation are approached. Whether these results are a fluke and whether $\alpha \to f/\bar{N}$ for all vortices that are created in one particular case is not yet clear. The physics governing these vortices is currently being investigated and will be discussed in a future paper.

Gill's relation for α, discussed in § 3, is not a good fit to any of our numerically computed vortices. For example, the value of $\alpha_{NUM}(t)/(Ro(t)f/\bar{N})$ is between 2 and 8 for case A1, 2 and 9 for case A8, 80 and 160 for case A20 and 4 and 7 for case B1. The much larger error observed for case A20 is due to the fact that unlike the other three cases, N_c is far from 0 in this case, and Gill's derivation does not incorporate $N_c \neq 0$.

8. Conclusion

We have derived a new relationship (2.9) for the aspect ratio α of baroclinic vortices in CG-H equilibrium and used numerical initial-value simulations of the Boussinesq equations to validate this relation for a wide variety of unforced quasi-steady vortices generated and dissipated with different mechanisms. Our new relationship shows that α depends on the background flow's Coriolis parameter f and Brunt–Väisälä

frequency $\bar{N}$, as well as properties of the vortex, including Ro and N_c. Thus, it shows that all vortices embedded in the same background flow do not have the same aspect ratios. In a companion paper, Aubert *et al.* (2012) verify the new relationship with laboratory experiments and show it to be consistent with observations of Atlantic meddies and Jovian vortices.

Equation (2.9) for α has several consequences. For example, it shows that for cyclones ($Ro > 0$), N_c must be greater than $\bar{N}$, that is, the fluid within a cyclone must be super-stratified with respect to the background stratification. Mixing usually de-stratifies the flow over a local region, and therefore cannot produce cyclones. This may explain why there are more anticyclones than cyclones observed in nature. We numerically simulated local suction to create cyclones, and we found that suction creates a large envelope of super-stratified flow around the location of the suction and when the suction is stopped, the CG-H adjustment makes cyclones. Details of these simulations and results of an ongoing laboratory experiment will be presented in subsequent publications.

It is widely quoted that vortices obey the quasi-geostrophic scaling law $\alpha = f/\bar{N}$ (i.e. Burger number $Bu = 1$). This is inconsistent with our relationship which written in terms of Bu is $Bu = Ro(1 + Ro)/[(N_c/\bar{N})^2 - 1]$. We found that, with the exception of one family of vortices, the quasi-geostrophic scaling law was not obeyed by the vortices studied here (and by Aubert *et al.* 2012), and could be incorrect by more than a factor of 10. Another relationship proposed by Gill (1981) was also found to produce very poor predictions of aspect ratio.

We found that α can either increase or decrease as the vortex decays, and our relationship (2.9) shows that the dependence of α on N_c is specially sensitive when N_c is at the order of $\bar{N}$, as it is for meddies and Jovian vortices (Aubert *et al.* 2012). Our simulations showed that N_c was determined by the secondary circulations within a vortex and that those circulations are controlled by the dissipation. In a future paper we shall report on the details of how dissipation determines the secondary flows and the temporal evolution of N_c, both of which are important in planetary atmospheres, oceanic vortices, accretion disc flows and planet formation (Barranco & Marcus 2005).

Acknowledgements

This work used an allocation of computer resources from the Extreme Science and Engineering Discovery Environment (XSEDE), which is supported by National Science Foundation grant number OCI-1053575. We also thank Dr C.-H. Jiang for his help with developing the numerical code. We acknowledge support from the NSF AST and ATI Programs, and from the NASA Planetary Atmospheres Program. P.H. was supported in part by the Natural Sciences and Engineering Research Council of Canada through a PGS-D scholarship. P.S.M. thanks the France-Berkeley Fund and Ecole Centrale Marseille. P.L.G. thanks the Russel Severance Springer Professorship endowment and the Planetology National Program (INSU, CNRS).

REFERENCES

Armi, L., Hebert, D., Oakey, N., Price, J. F., Richardson, P. L., Rossby, H. T. & Ruddick, B. 1988 The history and decay of a Mediterranean salt lens. *Nature* **333** (6174), 649–651.

Aubert, O., Le Bars, M., Le Gal, P. & Marcus, P. S. 2012 The universal aspect ratio of vortices in rotating stratified flows: experiments and Observations. *J. Fluid Mech.* **706**, 34–45.

BARCILON, V. & PEDLOSKY, J. 1967 On the steady motions produced by a stable stratification in a rapidly rotating fluid. *J. Fluid Mech.* **29**, 673–690.

BARRANCO, J. A. & MARCUS, P. S. 2005 Three-dimensional vortices in stratified protoplanetary disks. *Astrophys. J.* **623** (2), 1157–1170.

BARRANCO, J. A. & MARCUS, P. S. 2006 A 3D spectral anelastic hydrodynamic code for shearing, stratified flows. *J. Comput. Phys.* **219** (1), 21–46.

BILLANT, P. & CHOMAZ, J.-M. 2001 Self-similarity of strongly stratified inviscid flows. *Phys. Fluids* **13** (6), 1645–1651.

CARTON, X. 2001 Hydrodynamical modeling of oceanic vortices. *Surv. Geophys.* **22** (3), 79–263.

CHARNEY, J. G. 1971 Geostrophic turbulence. *J. Atmos. Sci.* **28**, 1087–1095.

DRITSCHEL, D. G., JUAREZ, M. D. & AMBAUM, M. H. P. 1999 The three-dimensional vortical nature of atmospheric and oceanic turbulent flows. *Phys. Fluids* **11** (6), 1512–1520.

GENT, P. R. & MCWILLIAMS, J. C. 1986 The instability of barotropic circular vortices. *Geophys. Astrophys. Fluid Dyn.* **35**, 209–233.

GILL, A. E. 1981 Homogeneous intrusions in a rotating stratified fluid. *J. Fluid Mech.* **103**, 275–295.

HUMPHREYS, T. & MARCUS, P. S. 2007 Vortex street dynamics: the selection mechanism for the areas and locations of Jupiter's vortices. *J. Atmos. Sci.* **64** (4), 1318–1333.

MARCUS, P. S. 1993 Jupiter's Great Red Spot and other vortices. *Annu. Rev. Astron. Astrophys.* **31**, 523–573.

MCWILLIAMS, J. C. 1985 Submesoscale, coherent vortices in the ocean. *Rev. Geophys.* **23** (2), 165–182.

MCWILLIAMS, J. C. 1988 Vortex generation through balanced adjustment. *J. Phys. Oceanogr.* **18** (8), 1178–1192.

MCWILLIAMS, J. C., WEISS, J. B. & YAVNEH, I. 1994 Anisotropy and coherent vortex structures in planetary turbulence. *Science* **264** (5157), 410–413.

MCWILLIAMS, J. C., WEISS, J. B. & YAVNEH, I. 1999 The vortices of homogeneous geostrophic turbulence. *J. Fluid Mech.* **401**, 1–26.

MOREL, Y. & MCWILLIAMS, J. 1997 Evolution of isolated interior vortices in the ocean. *J. Phys. Oceanogr.* **27** (5), 727–748.

NOF, D. 1981 On the β-induced movement of isolated baroclinic eddies. *J. Phys. Oceanogr.* **11** (12), 1662–1672.

DE PATER, I., WONG, M. H., MARCUS, P., LUSZCZ-COOK, S., ADAMKOVICS, M., CONRAD, A., ASAY-DAVIS, X. & GO, C. 2010 Persistent rings in and around Jupiter's anticyclones – observations and theory. *Icarus* **210** (2), 742–762.

REINAUD, J. N., DRITSCHEL, D. G. & KOUDELLA, C. R. 2003 The shape of vortices in quasi-geostrophic turbulence. *J. Fluid Mech.* **474**, 175–192.

SAYANAGI, K. M., MORALES-JUBERIAS, P. & INGERSOLL, A. P. 2010 Saturn's Northern Hemisphere Ribbon: simulations and comparison with the meandering Gulf Stream. *J. Atmos. Sci.* **67** (8), 2658–2678.

SHETTY, S. & MARCUS, P. S. 2010 Changes in Jupiter's Great Red Spot (1979–2006) and Oval BA (2000–2006). *Icarus* **210** (1), 182–2018.

SMYTH, W. D. & MCWILLIAMS, J. C. 1998 Instability of an axisymmetric vortex in a stably stratified, rotating environment. *Theor. Comput. Fluid Dyn.* **11** (3–4), 305–322.

STUART, G. A., SUNDERMEYER, M. A. & HEBERT, D. 2011 On the geostrophic adjustment of an isolated lens: dependence on burger number and initial geometry. *J. Phys. Oceanogr.* **41** (4), 725–741.

VALLIS, G. K. 2006 *Atmospheric and Oceanic Fluid Dynamics*. Cambridge University Press.

VAN HEIJST, G. J. F. & KLOOSTERZIEL, R. C. 1989 Tripolar vortices in a rotating fluid. *Nature* **338** (6216), 569–571.